Received: 9 July 2018 | Revised: 17 January 2019 | Accepted: 27 February 2019

DOI: 10.1002/asl.894

Atmospheric Science Letters RMetS

RESEARCH ARTICLE

A 14-year statistics-based semi-idealized modeling study on the formation of a type of heavy rain–producing southwest vortex

Yuan-Chun Zhang[1] | Shen-Ming Fu[2] | Jian-Hua Sun[1,3] | Rui Fu[4] | Shuang-Long Jin[5] | Dong-Sheng Ji[6]

[1]Laboratory of Cloud–Precipitation Physics and Severe Storms, Institute of Atmospheric Physics, Chinese Academy of Sciences, Beijing, China

[2]International Center for Climate and Environment Sciences, Institute of Atmospheric Physics, Chinese Academy of Sciences, Beijing, China

[3]State Key Laboratory of Severe Weather, Chinese Academy of Meteorological Sciences, Beijing, China

[4]Yunnan Research Institute of Meteorology, Yunnan Meteorological Bureau, Kunming, China

[5]State Key Laboratory of Operation and Control of Renewable Energy & Storage Systems, China Electric Power Research Institute, Beijing, China

[6]State Key Laboratory of Atmospheric Boundary Layer Physics and Atmospheric Chemistry, Institute of Atmospheric Physics, Chinese Academy of Sciences, Beijing, China

Correspondence
Shenming Fu, International Center for Climate and Environment Sciences, Institute of Atmospheric Physics, Chinese Academy of Sciences, Beijing 100029, China.
Email: fusm@mail.iap.ac.cn

Funding information
This research was supported by the Strategic Priority Research Program of Chinese Academy of Sciences (Grant/Award Number: XDA17010105), the Key R&D Program of Jiangxi Province of China (Grant/Award Number: 20171BBG70005), the Science Technology Foundation of State Grid Corporation of China (Grant/Award Number: NYB17201800148), the National Key R&D Program of China (Grant/Award Number: 2018YFC0809400), and the National Natural Science Foundation of China (Grant/Award Number: 41775046).

On the basis of a 14-year statistical dataset of the southwest vortex (SWV), 10 long-lived and heavy rain–producing SWVs are selected for a series of convection-permitting composite semi-idealized simulations. After confirming the simulation has reproduced the common salient features of these selected vortices, the general underlying mechanisms for the formation of this type of SWV are investigated. Results show that the SWV formation is characterized by significant unevenness, as the fundamental characteristics and dominant factors for the cyclonic-vorticity production vary from place to place. Overall, the eastern/western section of SWV mainly features favorable/unfavorable conditions for the cyclonic-vorticity enhancement. The vorticity budget indicates the convergence-related horizontal shrinking and convection-related tilting contribute to the cyclonic-vorticity enhancement in the SWV's eastern section, whereas in the western section, the terrain-related tilting and horizontal transport result in the cyclonic-vorticity reduction.

KEYWORDS
heavy rainfall, semi-idealized simulation, southwest vortex, vorticity budget

1 | INTRODUCTION

Every year, the high-impact weather, such as torrential precipitation, thunderstorms, and strong winds, results in considerable socioeconomic damage and heavy human casualties worldwide. In China, the torrential precipitation accounts for the largest proportion of the losses (Wu *et al.,* 2014). The torrential precipitation–related disasters, such as flash floods, urban waterlogging, landslides, and mudslides, usually occur in the warm season (i.e., from April to October) (Zhao *et al.,* 2004), during which the rainfall is frequent and the precipitation is heavy.

There are three major rain areas in China: south China, the Yangtze–Huaihe River basin, and north China (Tao, 1980). Atmospheric systems accounting for precipitation in these three areas show distinctive features. For the Yangtze–

Huaihe River basin, mesoscale vortices are one of the most important rainfall systems (Lu, 1986; Zhao *et al.,* 2004; Fu *et al.,* 2014). These mesoscale vortices mainly originate from two regions: the Sichuan Basin east of the Tibetan Plateau (TP) and the Dabie Mountain (Zhang *et al.,* 2015; Fu *et al.,* 2016) east of the Sichuan Basin. In China, the former is defined as the southwest vortex (SWV; Lu, 1986).

For decades, the mechanisms underlying the SWV formation are a research hotspot. For instance, Gao (1987) found that shallow warm and moist air in the lower troposphere makes a contribution to the SWV formation using a two-layer model. Kuo *et al.* (1988) investigated the SWV that induced the famous 1981 Sichuan flood event. They found that the vortex formed within the southwesterly monsoon flow, remote from the baroclinic frontal system to the north. Qian *et al.* (1990) conducted sensitivity experiments on the same vortex and proposed that latent heating was the most important factor for its formation. In contrast, the SWV event documented by Zhao and Fu (2007) showed far less dependence on latent heating; rather, cold advection and friction around the Sichuan Basin made a larger contribution. Fu *et al.,* 2011; 2013; 2014) found that the SWV formation usually featured an increase in the kinetic energy of its horizontal peripheral wind field. This enhancement of kinetic energy was mainly due to the release of the available potential energy (i.e., the baroclinic energy conversion). Wang and Tan (2014) investigated the influences of the terrain features on the SWV formation and suggested that the Sichuan Basin only plays a secondary role in this process.

As mentioned above, previous studies have proposed several mechanisms that can lead to the formation of an SWV and, among them, from case to case, some factors are similar while others show distinct differences. This is similar to the situation in the mesoscale convective vortex (MCV) research (Zhang, 1992), that is, different cases show different features. This means that case studies may be limited to reflect the universal features of the mechanisms underlying the SWV formation. Thus, a composite analysis of the formation mechanisms is necessary (Fu *et al.,* 2014). As there are many types of SWVs (Lu, 1986; Fu *et al.,* 2014), we only focus on one typical SWV type that frequently induces heavy precipitation events around the Sichuan Basin (section 2). The primary purpose of this study is to reveal the common mechanisms accounting for the formation of this typical type of SWV.

The paper is structured as follows: the model configuration, semi-idealized simulation design, and the vorticity budget method are described in section 2; the main results and conclusions are provided in sections 3 and 4, respectively.

2 | METHODS

Recently, Fu *et al.* (2014) have conducted a 14-year (2000–2013) statistical analysis of SWVs, in which they classified these vortices into four categories, that is, the "no precipitation and no surface low," "surface low only," "precipitation only (PN)," and "precipitation and surface low" types. Because the PN type occupies the largest proportion (~51.1%) and has a high probability of inducing heavy precipitation (~97.2%) and thunderstorms (~70.4%) (Fu *et al.,* 2014), it is selected in this study as the typical SWV type for the semi-idealized simulation.

Among the PN type of SWVs documented by Fu *et al.* (2014), only 10 cases (Table 1) are used in the composite simulation. These events have four significant features in common: (a) their large-scale favorable background circulations for SWV formation (including the middle tropospheric shortwave trough, temperature field, and upper-level jet); (b) their long duration (>36 hr); (c) their quasi-stationary behavior; and (d) their associated heavy precipitation during their lifespans. The 6-hourly $0.5 \times 0.5^{\circ}$ Climate Forecast System Reanalysis data (CFSR; Saha *et al.,* 2010) is used to for simulations. The composite method documented in Fu *et al.* (2017) is used in this study: suppose a sample variable S at the formation time of each SWV is S_n (0), where n represents the number of vortices. The time series S_n (−2), S_n (−1), S_n (0), S_n (1), S_n (2), S_n (3), S_n (4), with an interval of 6-hr represents the period from 12 hr before the formation of a SWV n to 24 hr after its initiation (i.e., the simulation period is defined as from 12 hr before SWV formation to 24 hr after the vortex initiation to focus on SWV formation). For the 10 SWVs, the corresponding times were composited equally weighted under the Euler coordinate. This results an ideal 36-hr time series with a 6-hr interval, which is used as the initial and boundary conditions for the semi-idealized simulation. The simulation is initiated at 1800 UTC (0200 Beijing Standard Time [BST]), which is temporally around average for the 10 SWVs (Table 1). For this type of semi-idealized simulation, the composite may remove some small- and/or mesoscale information from the initial and boundary conditions for the simulation; therefore, it mainly focuses on the contribution of large-scale environmental circulations.

TABLE 1 Formation time, lifespans, and maximum 6-hr accumulated precipitation of the SWVs used in the composite semi-idealized simulation

No.	Formation time (UTC)	Life span (hr)	Maximum 6-hr precipitation (mm)
1	0600 UTC Jul 1, 2000	36	54
2	1200 UTC Jul 4, 2000	36	20
3	0600 UTC Aug 17, 2000	60	69
4	0600 UTC Jul 16, 2007	112	59
5	0000 UTC Jul 28, 2007	48	69
6	0600 UTC Jul 30, 2007	36	36
7	0000 UTC Jul 21, 2008	156	58
8	0600 UTC Aug 14, 2008	78	105
9	1200 UTC Aug 24, 2008	42	43
10	1800 UTC Jul 4, 2010	60	71

A single domain convection-permitting version (horizontal grid spacing: 4 km) of the Weather Research and Forecasting (WRF) model (Skamarock *et al.,* 2008), which has a domain of 1,021 (east–west) × 721 (north–south) × 51 (vertical levels) points (model top: 50 hPa). The Yonsei University planetary boundary layer scheme (Noh *et al.,* 2001), Noah land-surface model (Chen and Dudhia, 2001), and WRF single-moment 6-class microphysics scheme (Hong and Lim, 2006) are used in the semi-idealized simulation. No cumulus parameterization scheme is used, because the grid spacing of 4 km is convection-permitting.

Similar to previous studies (Zhang, 1992; Olsson and Cotton, 1997; Sun *et al*., 2010; Fu *et al.,* 2017), the vorticity budget is used here to understand the mechanisms of SWV formation. The equation documented in Kirk (2003) is as follows:

$$\frac{\partial \zeta}{\partial t} = \underbrace{-\mathbf{V}_h \cdot \nabla_h \zeta}_{\text{HAV}} \underbrace{-\omega \frac{\partial \zeta}{\partial p}}_{\text{VAV}} + \underbrace{\mathbf{k} \cdot \left(\frac{\partial \mathbf{V}_h}{\partial p} \times \nabla_h \omega \right)}_{\text{TIL}} \underbrace{-\beta v}_{\text{APV}} \underbrace{-(\zeta + f)\nabla_h \cdot \mathbf{V}_h}_{\text{STR}} + \text{RES}, \quad (1)$$

where ζ is relative vorticity, $\mathbf{V}_h = u\mathbf{i} + v\mathbf{j}$ is the horizontal wind vector, f is the Coriolis parameter, $\beta = \partial f/\partial y$, $\nabla_h = \frac{\partial}{\partial x}\mathbf{i} + \frac{\partial}{\partial y}\mathbf{j}$ is the horizontal gradient operator, p is pressure, and $\omega = dp/dt$. Terms HAV and VAV represent the horizontal and vertical advection of vorticity, respectively. TIL is tilting, APV denotes the advection of planetary vorticity, STR stands for stretching, and RES is the residual effect. Term TOT is defined as TOT = HAV + VAV + TIL + APV + STR, which is the total effect of the right-hand side terms, except for RES.

3 | RESULTS

3.1 | Validation of the simulation

The prime goal of the semi-idealized simulation is to reproduce the selected SWVs' commonality. Comparisons between Figures 1a,b and 2a,b show that the simulation reproduces the shortwave trough east of the TP, the warm tongue stretching out from the TP, and the 200-hPa upper-level jet northwest of the TP reasonably. This means that the characteristics of the large-scale background circulations for SWV formation are captured successfully. Moreover, the simulation also captures the main features of the lower-level stream field, ascending motions, temperature and precipitation of the composite reasonably (not shown). The simulated SWV forms at t = ~13 hr (i.e., after 13 hr of the model run), approximately 1 hr later than the composite SWV. The center of the simulated SWV is located ~150 km northeast of that of the composite vortex (cf., Figures 1b and 2b). This center-location difference between the simulation and composite is within the acceptable range, because it is only ~25% of the SWV's diameter. As shown in Figure 1c, obvious precipitation (maximum 9-hr accumulated precipitation is above 50 mm) appears before the SWV formation, while there is no closed surface low center. In terms of the classification criteria defined by Fu *et al.* (2014), the simulated SWV belongs to the PN type (i.e., precipitation only, introduced in section 2). The simulated SWV maintains a quasi-stationary behavior after formation and induces torrential precipitation during its lifespan (not shown), both of which are consistent with the common features of the selected SWVs (Table 1). In summary, although there are some detailed differences between the semi-idealized simulation and composite, the simulation reproduces the salient features of this type of SWV credibly. Thus, the simulation results can be used to represent this type of event.

3.2 | Overview of the simulated event

As Figure 2a,b illustrates, the upper-level jet is mainly located northwest of the TP, which has unobvious effects on the SWV formation. From t = 6 hr (0800 BST) to 12 hr (1400 BST), due to the increasing downwards shortwave radiation, the upwards sensible heat flux over the TP enhances, which intensifies the 500-hPa warm tongue, makes it enlarge eastward, and covers the Sichuan Basin. As a result, the regions around the Sichuan Basin experiences a pressure lowering (Markowski and Richardson, 2010), which contributes to occurrence/development of convection. A 500-hPa shortwave trough is located east of the TP and maintains a quasi-stationary behavior. The SWV forms ahead of this trough, where warm advection and cyclonic-vorticity advection appear (not shown). These two conditions enhance ascending motions via quasi-geostrophic forcing (Holton, 2004). According to Raymond and Jiang (1990), positive feedback exists among the convergence, ascending motion, and latent heating: as ascending motion enhances, convergence (favoring cyclonic-vorticity production) and latent heating (contributing to pressure reduction) intensify, both of which are conducive to the SWV formation.

A key region (29.5°–33.5°N, 104°–109°E) of the SWV, which covers the main body of the vortex, is defined as Figure 2d shows. It is used to investigate the SWV formation. A sensitivity test indicates that the calculation results averaged within this key region are insensitive to relatively small changes (±0.5° to each boundary line) (not shown). This means the key region can show

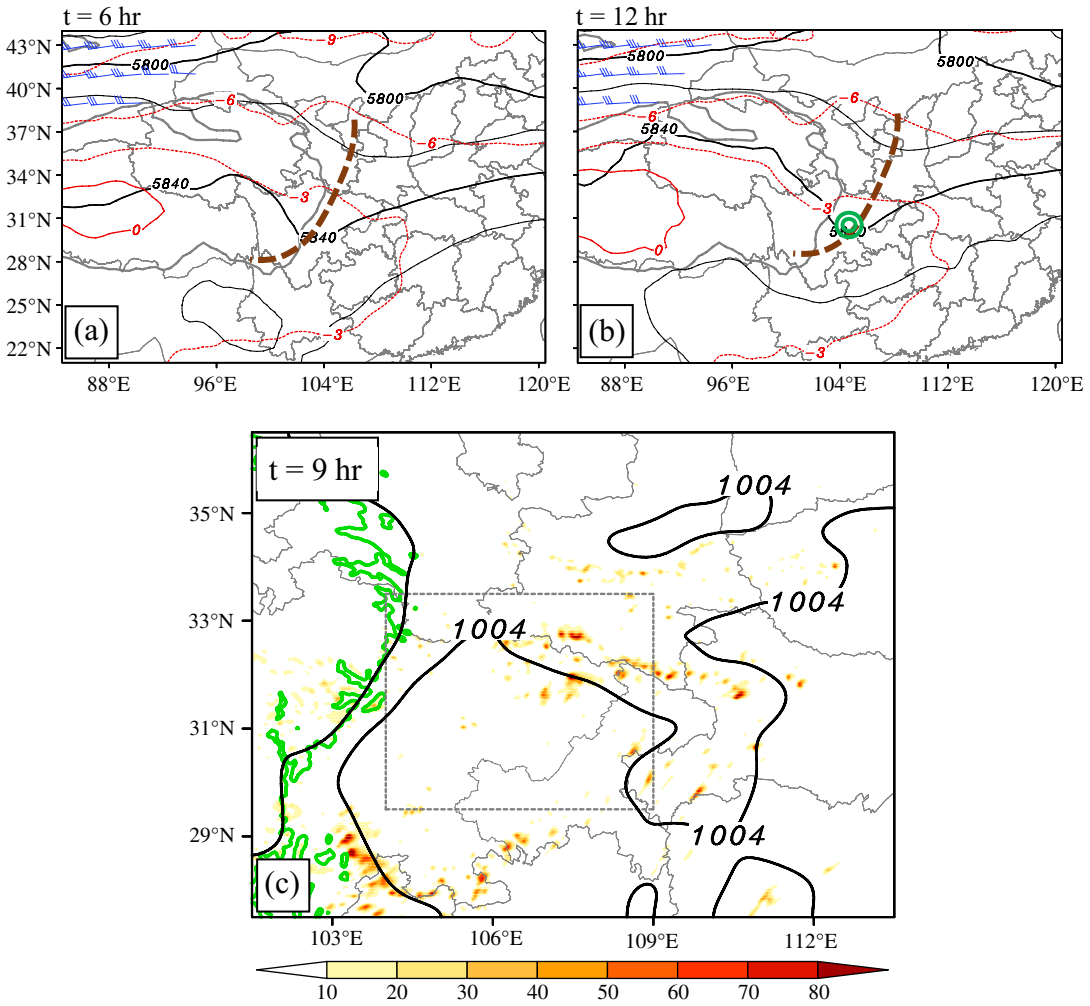

FIGURE 1 Panels (a, b) show the 200-hPa wind speed above 30 m/s (a full bar is 10 m/s), 500-hPa geopotential height (black lines, units: gpm), and 500-hPa temperature (red lines, units: °C) in the composite of 10 events (using FNL data), where the brown dashed line is the trough line, the thick gray line outlines terrain above 3,000 m, and the green concentric circles mark the initial location of the SWV. Panel (c) shows the 9-hr accumulated precipitation (shading, units: mm), and the sea level pressure (black line, units: hPa), where the green solid line outlines terrain above 3,000 m

relatively credible results. Because the key region–averaged vorticity maintains a strong intensity and shows an unobvious variational trend (not shown), we further divide this region into four even sections I–IV, along the vertical wind shear. From Figure 3, it can be found that similar to that documented in Fu *et al.* (2014), the key features within sections I–IV show significant unevenness: section IV has the largest cyclonic vorticity before t = 11 hr, followed by section I and then section II. In contrast, section III has the weakest cyclonic vorticity, with a slow decreasing trend. Ascending motion occurs mainly in sections I–III, whereas section IV is primarily dominated by descending motion. Sections I and II feature increasing convergence, whereas the air flow within sections III and IV mainly keep divergent. In summary, section I, which features rapid increasing cyclonic vorticity, is the most active section during the SWV formation. In contrast, sections III and IV are inactive, showing mainly opposite features. Mechanisms governing the inhomogeneous vorticity variation are discussed in the next section.

3.3 | Vorticity budget analysis

Equation 1 is used to investigate the mechanisms accounting for the evolution of vorticity associated with the SWV. The overall balance of this equation is good after ignoring the RES term (not shown) because, on average, term TOT can account for ~75% of the local time variation (calculated based on a central difference scheme using 15-min WRF output data). Vorticity budgets averaged within the key region are consistent with that reported by Fu *et al.* (2014): convergence-related STR dominates cyclonic-vorticity production, whereas horizontal advection (HAV) is the most important factor decelerating the SWV's formation. This also confirms that the simulated SWV is representative of the PN type of SWV. In addition, titling (TIL) and vertical transport (VAV), which are both closely related to convection, change their effects from t = 6 hr to

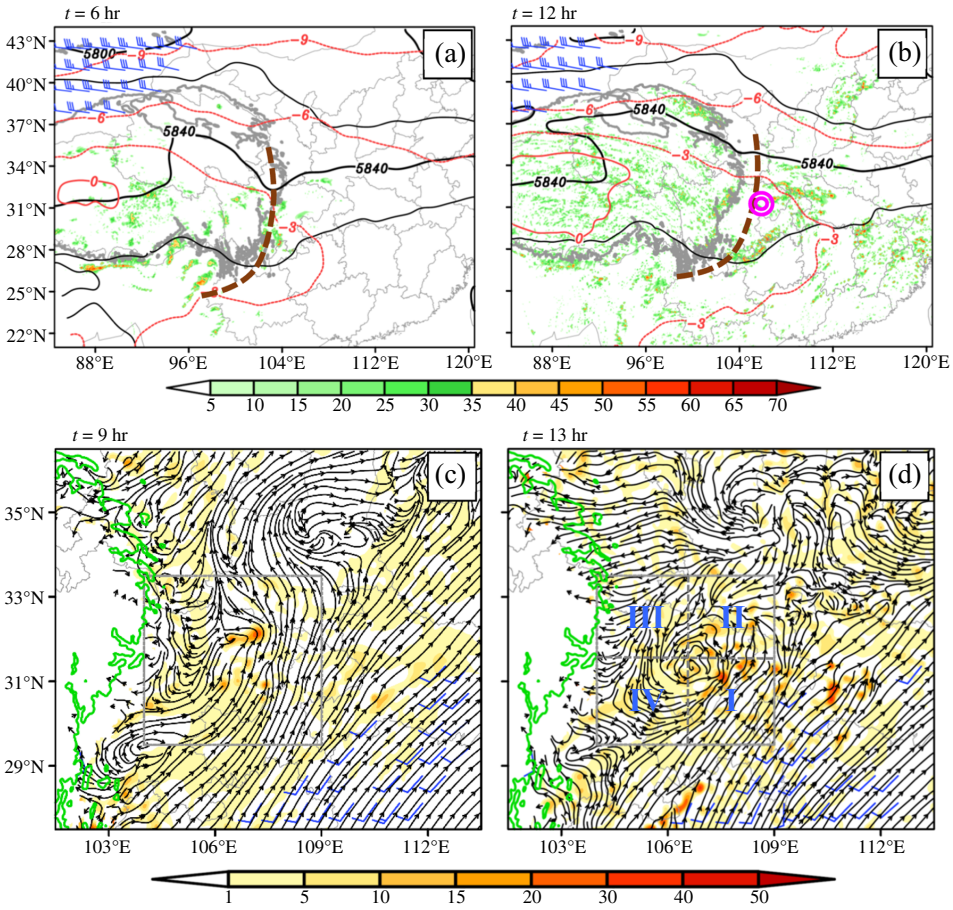

FIGURE 2 Panels (a, b) show the simulated 200-hPa wind speed above 30 m/s (a full bar is 10 m/s), 500-hPa geopotential height (black lines, units: gpm), 500-hPa temperature (red lines, units: °C), and composite reflectivity (shading, units: dBZ), where the brown dashed line represents the trough line, and the thick gray line marks terrain above 3,000 m. Panels (c, d) show the simulated vorticity (shading, units: 10^{-5} s^{-1}), stream field and wind speed above 6 m/s (a full bar is 6 m/s) at 700 hPa, where the green solid line outlines terrain above 3,000 m, and the gray box with crossed lines shows the key region of the SWV and sections I–IV

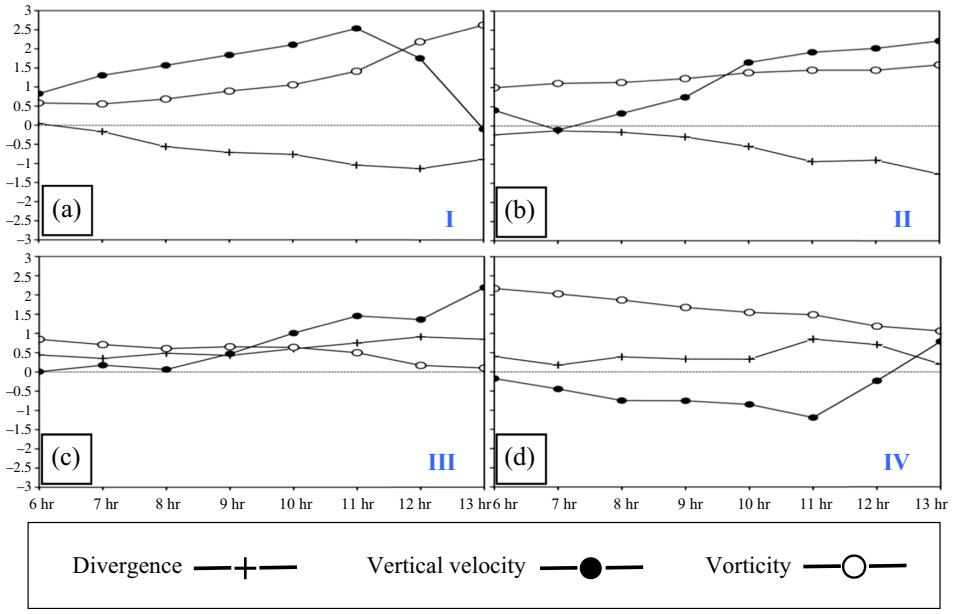

FIGURE 3 The horizontal averaged divergence (units: 10^{-5} s^{-1}), vertical velocity (units: m/s), and vorticity (units: 10^{-5} s^{-1}) within sections I–IV of the key region (Figure 2d), respectively

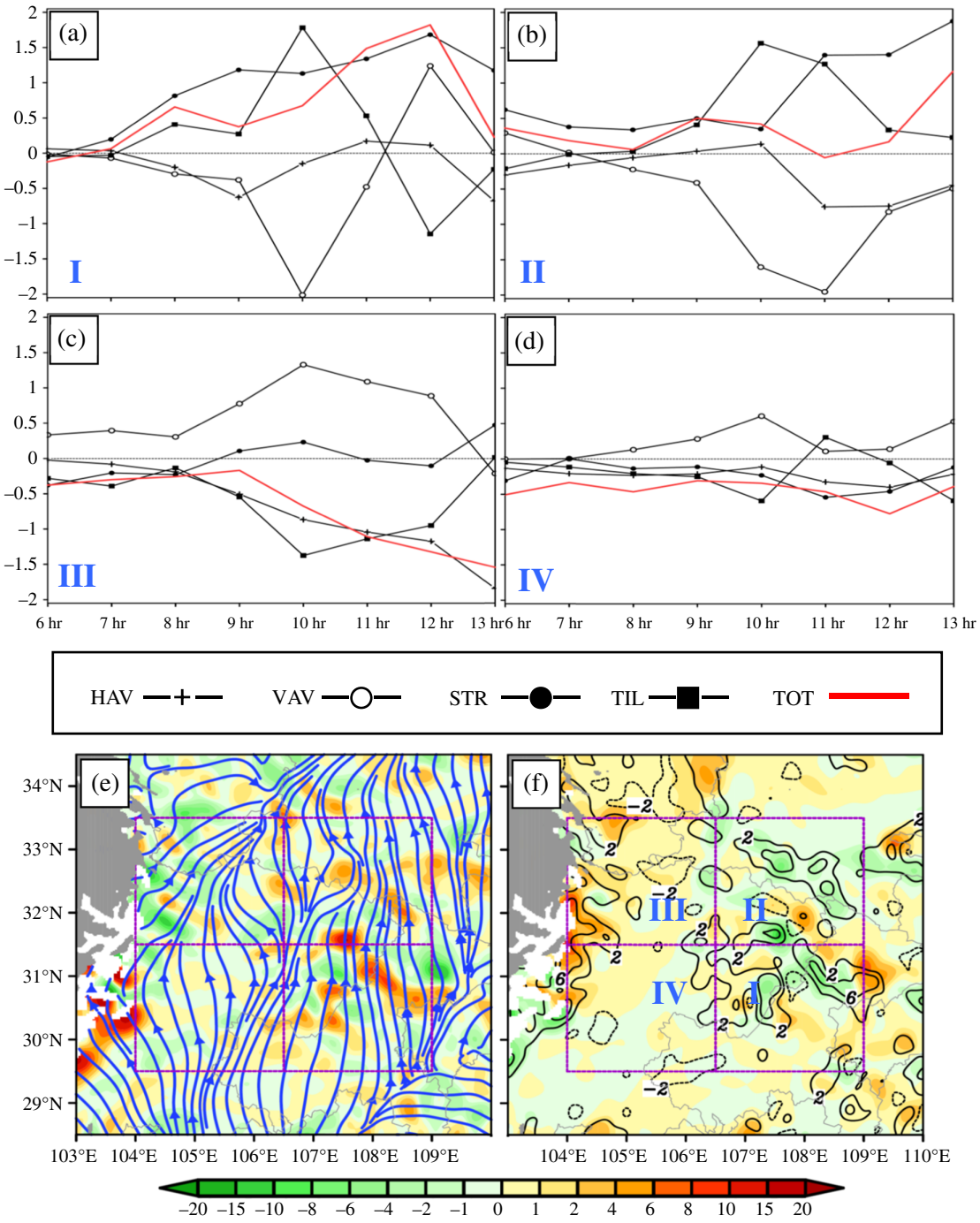

FIGURE 4 Panels (a, d) show the simulated horizontal averaged vorticity budget terms (units: 10^{-9} s^{-2}) within sections I–IV (Figure 2d), respectively. Panel (e) shows the time-mean (from t = 6 hr to 13 hr) horizontal vortex line (blue line; units: 10^{-3} s^{-1}), and TIL at 700 hPa (shading, units: 10^{-9} s^{-2}). Panel (f) shows the time-mean (from t = 6 hr to 13 hr) vertical velocity (dark lines, units: cm/s), and VAV at 700 hPa (shading, units: 10^{-9} s^{-2})

13 hr (not shown): TIL first accelerates the cyclonic-vorticity production and then decelerates it; whereas VAV experiences an opposite variation to that of the TIL. However, in total, their effects are only of secondary importance.

Compared to the total result averaged within the key region, each section shows distinctive characteristics. For section I, which features the most rapid enhancement in cyclonic vorticity (Figure 3a), term TOT is also largest (Figure 4a). As Figure 2c,d illustrates, the southeast of section I maintains a low-level jet. In the northern terminus of this jet, convergence and ascending motion are strong (Figures 2b, 3a, and 4f). Under these two favorable conditions, the convergence-related horizontal shrinking (i.e., STR) and the tilting that is closely related to convection (i.e., TIL) act as the most and second-most important factors, respectively, contributing to the cyclonic-vorticity production. From Figure 4e, the horizontal vortex lines mainly stretch from south to north around sections I and II. As documented by Markowski and Richardson (2010), the

horizontal vorticity vector $= \left(\frac{\partial w}{\partial y} - \frac{\partial v}{\partial z}\right)\mathbf{i} + \left(\frac{\partial u}{\partial z} - \frac{\partial w}{\partial x}\right)\mathbf{j} \approx -\frac{\partial v}{\partial z}\mathbf{i} + \frac{\partial u}{\partial z}\mathbf{j}$, where ($u$, v, w) are the three-dimensional wind component in the (x, y, z) directions. As the meridional component is dominant (Figure 4e), $\left|\frac{\partial u}{\partial z}\mathbf{j}\right|$ is much larger than $\left|-\frac{\partial v}{\partial z}\mathbf{i}\right|$, or in other words, the horizontal vortex lines around sections I and II are mainly determined by the zonal wind vertical shear. Because these vortex lines are at 700 hPa (~3,000 m), which is much higher than the underlying topography, tilting in this region is mainly due to vertical motion (Figure 4f), instead of terrain lifting. However, it should be noted that terrain can modify vertical motion, thus affecting tilting indirectly. Although ascending motion dominates section I (Figure 3a), the vertical transport of vorticity (VAV) acts as the most detrimental factor for the SWV formation. This is because the levels of 850–700 hPa have smaller cyclonic vorticity than 700–550 hPa (not shown); thus, ascending motion transports relatively weaker cyclonic vorticity upward to the SWV's central level which replaces the stronger one. Horizontal transport of vorticity (HAV) has different effects in different regions: It mainly imports cyclonic vorticity via the western and southern boundaries of section I, while the export of cyclonic vorticity occurs via the northern and eastern boundaries (not shown). In total, HAV makes a negative contribution to the SWV formation (Figure 4a), as it overall causes a net export of cyclonic vorticity from the key region.

Section II shows similar features to those in section I (cf., Figure 3a,b), but smaller in intensity. Its increasing trend of cyclonic vorticity is smaller than that in section I (cf., Figure 4a,b). Convergence-related horizontal shrinking and convection-related tilting again act as favorable factors for the increase in cyclonic vorticity (Figure 4b), whereas compared to that in section I, TIL makes a larger relative contribution. Moreover, tilting has similar features to those in section I, that is, its meridional stretching vortex lines are mainly tilted by vertical motion, instead of terrain (Figure 4e,f). Relatively, ascending motion transports smaller quantities of cyclonic vorticity upward (not shown), which decelerates the increase in cyclonic vorticity (Figure 4b). The horizontal advection also makes a negative contribution, mainly through exporting cyclonic vorticity via the northern and western boundaries of section II (not shown). The cyclonic vorticity imported (from section I) via the southern boundary of section II offsets a part of the negative HAV in section II.

Sections III and IV feature a negative TOT (Figure 4c,d), that is, conditions are unfavorable for maintaining cyclonic vorticity. This is consistent with the decreasing trends of cyclonic vorticity in these regions (Figure 3c,d). For section III, horizontal transport and tilting dominate the reduction in cyclonic vorticity (Figure 4c), and the divergence-related horizontal stretching (i.e., STR) also contributes to this decrease; whereas, the upward transport of relatively stronger cyclonic vorticity mainly acts as resisting the cyclonic-vorticity decreasing. Section IV has similar evolutionary factors to those in section III (i.e., HAV, TIL and VAV), but weaker in intensity (cf., Figure 4c,d). Compared to section III, divergence-related horizontal stretching (Figure 3d) is stronger in section IV, which also acts as a dominant factor for its decrease in cyclonic vorticity (Figure 4d). From Figure 4e, it can be seen that the southwest–northeast stretching vortex lines (indicating the meridional and zonal wind shear are of similar importance) appear in the western part of sections III and IV, particularly for section III, where stronger tilting appears (cf., Figure 4c, d). The high terrain (>3,000 m) on the eastern flank of the TP (around 104°E) has a lifting effect on these vortex lines, which produces negative vorticity (Figure 4e). This can be verified by the strong negative tilting (i.e., TIL) in the western part of sections III and IV. The horizontal transport (i.e., HAV) reduces the cyclonic vorticity in these sections, which mainly exports cyclonic vorticity through the northern and southern boundaries of section III, as well as the western and eastern boundaries of section IV (not shown).

4 | CONCLUDING REMARKS

In this study, based on a 14-year statistical study of SWVs (Fu *et al.,* 2017), 10 typical SWVs are selected for a semi-idealized simulation (Fu *et al.,* 2016). All the selected vortices are long-lived, have quasi-stationary behaviors, and induce heavy precipitation during their lifespans (Table 1). Moreover, in terms of the classification criteria of Fu *et al.* (2014), all these vortices belong to the PN type. The semi-idealized simulation based on the composite of these 10 SWVs produces a PN-type SWV that captures the salient characteristics of these 10 events, including the large-scale background circulations, precipitation, initiation time/locations, and quasi-stationary behaviors, as well as the dominant factors for their formation. This guarantees the

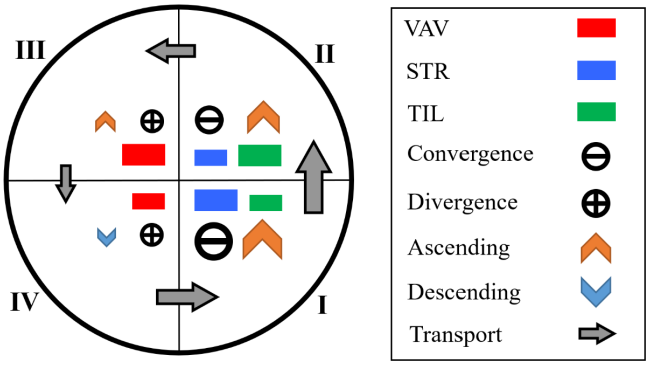

FIGURE 5 Schematic illustration of the key characteristics and dominant factors (contributing to the enhancement/sustainment of cyclonic vorticity) during the SWV formation, where the gray shaded arrows show the transport of cyclonic vorticity across the boundary lines of sections I–V. A bigger size of a sign means a larger intensity

simulated vortex can be used as a representative for this type of SWV.

Synoptic analysis shows that the middle-level warm tongue, which is mainly due to strong upward sensible heat flux over the TP, stretches out from the plateau and contributes to the SWV formation through a lower-level pressure reduction. The mid-tropospheric leeside shortwave trough east of the TP maintains a quasi-stationary behavior. The warm advection and cyclonic-vorticity advection ahead of this trough are conducive to the SWV formation through the increase of ascending motion and its associated positive feedback (Raymond and Jiang, 1990).

Similar to those documented in Fu *et al*. (2014), the formation of this PN-type SWV shows significant unevenness. Overall, the convergence-related horizontal shrinking and horizontal transport act as the most favorable and unfavorable factors, respectively, for maintaining cyclonic vorticity associated with the SWV. Most of the previous studies also confirm the convergence-related shrinking is a dominant factor for the SWV formation, whereas in some situations, the vertical transport (Lu, 1986; Fu *et al.,* 2015), and tilting (Wang and Tan, 2014) can also have a dominant effect. For the most detrimental factors, except for the horizontal transport, sometimes, the tilting is also dominant (Fu *et al.,* 2013; 2015). Within each section of the vortex, the key features and dominant factors for the variation in vorticity are distinct. Overall, a schematic illustration of the formation of a PN-type SWV is presented in Figure 5. Sections I and II are active areas during the SWV formation. They mainly feature ascending motion, convergence, and increasing cyclonic vorticity. Convergence-related horizontal shrinking and convection-related tilting govern the increase of cyclonic vorticity (shown in sections I–II in Figure 5). Tilting is mainly due to vertical motion (which is closely related to the lower-level jet), instead of terrain lifting. For these two sections, upward transport of relatively smaller cyclonic vorticity acts as the most important factor decelerating the increase in cyclonic vorticity.

Sections III and IV feature divergence and a decreasing trend of cyclonic vorticity (shown in sections III–IV in Figure 5). For section III, horizontal transport and tilting dominate the decrease in cyclonic vorticity, whereas vertical transport contributes to the cyclonic-vorticity maintenance (shown in section III in Figure 5). Section IV has similar governing factors to those in section III, but weaker in intensity (shown in section IV in Figure 5); moreover, divergence-related horizontal stretching also acts as a dominant factor for reducing cyclonic vorticity. For sections III and IV, negative tilting appears to be mainly due to the terrain lifting (around the eastern flank of the TP). This is significantly different from that within sections I and II. Overall, the horizontal transport exports cyclonic vorticity from the key region, which decelerates the increase in cyclonic vorticity associated with the vortex.

ACKNOWLEDGEMENTS

The authors thank the National Centers for Environmental Prediction and the China Meteorological Administration for providing the data. This research was supported by the Strategic Priority Research Program of Chinese Academy of Sciences (Grant No. XDA17010105), the Key R&D Program of Jiangxi Province of China (Grant No. 20171BBG70005), the Science Technology Foundation of State Grid Corporation of China (Grant No. NYB17201800148), the National Key R&D Program of China (Grant No. 2018YFC0809400), and the National Natural Science Foundation of China (Grant No. 41775046).

REFERENCES

Chen, F. and Dudhia, J. (2001) Coupling an advanced land surface–hydrology model with the Penn State–NCAR MM5 modeling system. Part I: Model implementation and sensitivity. *Monthly Weather Review*, 129, 569–585.

Fu, S.M., Li, W.L., Sun, J.H., Zhang, J.P. and Zhang, Y.C. (2015) Universal evolution mechanisms and energy conversion characteristics of long-lived mesoscale vortices over the Sichuan Basin. *Atmospheric Science Letters*, 16, 127–134.

Fu, S.M., Sun, J.H., Luo, Y.L. and Zhang, Y.C. (2017) Formation of long-lived summertime mesoscale vortices over central east China: semi-idealized simulations based on a 14-year vortex statistic. *Journal of the Atmospheric Sciences*, 74, 3955–3979.

Fu, S.M., Sun, J.H., Zhao, S.X. and Li, W.L. (2011) The energy budget of a southwest vortex with heavy rainfall over south China. *Advances in Atmospheric Sciences*, 28(3), 709–724.

Fu, S.M., Yu, F., Wang, D.H. and Xia, R.D. (2013) A comparison of two kinds of eastward-moving mesoscale vortices during the mei-yu period of 2010. *Science China Earth Sciences*, 56, 282–300.

Fu, S.M., Zhang, J.P., Sun, J.H. and Shen, X.Y. (2014) A fourteen-year climatology of the southwest vortex in summer. *Atmospheric and Oceanic Science Letters*, 7, 510–514.

Fu, S.M., Zhang, J.P., Sun, J.H. and Zhao, T.B. (2016) Composite analysis of long-lived mesoscale vortices over the middle reaches of the Yangtze River valley: octant features and evolution mechanisms. *Journal of Climate*, 29, 761–781.

Gao, S.T. (1987) The dynamic action of the disposition of the fluid fields and the topography on the formation of the south-west vortex. *Chinese Journal of Atmospheric Sciences*, 11, 263–271.

Holton, J.R. (2004) *An Introduction to Dynamic Meteorology*. San Diego: Academic Press.

Hong, S.Y. and Lim, J.O. (2006) The WRF single-moment microphysics scheme (WSM6). *Journal of Korean Meteorological Society*, 42, 129–151.

Kirk, J.R. (2003) Comparing the dynamical development of two mesoscale convective vortices. *Monthly Weather Review*, 131, 862–890.

Kuo, Y., Cheng, L. and Bao, J. (1988) Numerical simulation of the 1981 Sichuan flood. Part I: evolution of a mesoscale southwest vortex. *Monthly Weather Review*, 116, 2481–2504.

Lu, J.H. (1986) *Generality of the Southwest Vortex*. Beijing: China Meteorological Press.

Markowski, P. and Richardson, Y. (2010) *Mesoscale Meteorology in Midlatitudes*. Hoboken, NJ: Wiley-Blackwell.

Noh, Y., Cheon, W.G., and Raasch, S. (2001) The improvement of the K-profile model for the PBL using LES. In: Preprints of the International Workshop of Next Generation NWP Model, Seoul, South Korea, pp. 65–66.

Olsson, P.Q., and Cotton, W.R. (1997) Balanced and unbalanced circulations in a primitive equation simulation of a midlatitude MCC. Part II: Analysis of balance. *Journal of the Atmospheric Sciences*, 54, 479–497. https://doi.org/10.1175/1520-0469(1997)054,0479:BAUCIA.2.0.CO;2

Qian, Z.A., Gu, H.D., Yan, H., Chen, Y.C. and Li, S.H. (1990) Numerical simulations of extremely intense rainstorm and southwest vortex over Sichuan in July of 1981. *Acta Meteorologica Sinica*, 48, 415–423.

Raymond, D. and Jiang, H. (1990) A theory for long-lived mesoscale convective systems. *Journal of the Atmospheric Sciences*, 47, 3067–3077.

Saha, S., Moorthi, S., Pan, H.L., Wu, X.G., Wang, J.D., Nadiga, S., Tripp, P., Kistler, R., Woollen, J., Behringer, D., Liu, H.X., Stokes, D., Grumbine, R., Gayno, G., Wang, J., Hou, Y.T., Chuang, H.Y., Juang, H.M.H., Sela, J., Iredell, M., Treadon, R., Kleist, D., Delst, P.V., Keyser, D., Derber, J., Michael, E., Meng, J., Wei, H.L., Yang, R.Q., Lord, S., Dool, H.V.D., Kumar, A., Wang, W.Q., Long, C., Chelliah, M., Xue, Y., Huang, B.Y., Schemm, J.K., Ebisuzaki, W., Lin, R., Xie, P.P., Chen, M.Y., Zhou, S.T., Higgins, W., Zou, C.Z., Liu, Q.H., Chen, Y., Han, Y., Cucurull, L., Reynolds, R.W., Rutledge, G., and Goldberg, M. (2010) The NCEP climate forecast system reanalysis. *Bulletin of the American Meteorological Society*, 91, 1015–1057. https://doi.org/10.1175/2010BAMS3001.1

Skamarock, W.C., Klemp, J.B., Dudhia, J., Gill, D.O., Barker, D.M., Duda, M. G., Huang, X.Y., Wang, W., and Powers, J.G. (2008) A description of the advanced research WRF version 3. Boulder, CO NCAR. Technical note CAR/TN-475+STR, 113 pp.

Sun, J.-H., Zhao, S.-X., Xu, G.-K., and Meng, Q.-T. (2010) Study on a mesoscale convective vortex causing heavy rainfall during the mei-yu season in 2003. *Advances in Atmospheric Sciences*, 27, 1193–1209. https://doi.org/10.1007/s00376-009-9156-6

Tao, S.Y. (1980) *Rainstorms in China*. Beijing: Science Press.

Wang, Q.W. and Tan, Z.M. (2014) Multi-scale topographic control of southwest vortex formation in Tibetan Plateau region in an idealized simulation. *Journal of Geophysical Research: Atmospheres*, 119, 11543–11561.

Wu, J.D., Fu, Y., Zhang, J. and Li, N. (2014) Meteorological disaster trend analysis in China: 1949–2013. *Journal of Natural Resources*, 29, 1520–1530.

Zhang, D.L. (1992) The formation of a cooling-induced mesovortex in the trailing stratiform region of a midlatitude squall line. *Monthly Weather Review*, 120, 2763–2785.

Zhang, J.P., Fu, S.M., Sun, J.H., Shen, X.Y. and Zhang, Y.C. (2015) A statistical and compositional study on the two types of mesoscale vortices over the Yangtze River basin. *Climatic and Environmental Research*, 20, 319–336.

Zhao, S.X. and Fu, S.M. (2007) An analysis on the southwest vortex and its environment fields during heavy rainfall in eastern Sichuan Province and Chongqing in September 2004. *Chinese Journal of Atmospheric Sciences*, 31, 1059–1075.

Zhao, S.X., Tao, Z.Y., Sun, J.H. and Bei, N.F. (2004) *Study on Mechanism of Formation and Development of Heavy Rainfalls on Meiyu Front in Yangtze River*. Beijing: China Meteorological Press.

How to cite this article: Zhang Y-C, Fu S-M, Sun J-H, Fu R, Jin S-L, Ji D-S. A 14-year statistics-based semi-idealized modeling study on the formation of a type of heavy rain–producing southwest vortex. *Atmos Sci Lett*. 2019;e894. https://doi.org/10.1002/asl.894